Dynamical mean-field theory for the Bose-Hubbard model

Wen-Jun Hu and Ning-Hua Tong*
Department of Physics, Renmin University of China, Beijing 100872, People's Republic of China
(Received 20 March 2009; revised manuscript received 18 October 2009; published 11 December 2009)

The dynamical mean-field theory (DMFT), which is successful in the study of strongly correlated fermions, was recently extended to boson systems [K. Byczuk and D. Vollhardt, Phys. Rev. B **77**, 235106 (2008)]. In this paper, we employ the bosonic DMFT to study the Bose-Hubbard model which describes on-site interacting bosons in a lattice. Using exact diagonalization as the impurity solver, we get the DMFT solutions for the Green's function, the occupation density, as well as the condensate fraction on a Bethe lattice. Various phases are identified: the Mott insulator, the Bose-Einstein condensed (BEC) phase, and the normal phase. At finite temperatures, we obtain the crossover between the Mott-type regime and the normal phase, as well as the BEC-to-normal phase transition. Phase diagrams on the μ/U-$\tilde{t}/U$ plane and on the T/U-$\tilde{t}/U$ plane are produced ($\tilde{t}$ is the scaled hopping amplitude). We compare our results with the previous ones, and discuss the implication of these results to experiments.

DOI: 10.1103/PhysRevB.80.245110 PACS number(s): 71.10.Fd, 67.85.Hj, 03.75.Hh, 05.30.Jp

I. INTRODUCTION

The ultracold atoms trapped in an optical lattice have aroused growing interests in recent years. By regulating the various parameters of the standing-wave laser fields that create the optical potentials, such as the laser power and wavelength, many theoretical models in the condensed-matter physics can be realized experimentally, especially those for the strongly correlated many-body systems.[1] In particular, bosons in a lattice have been widely studied in theory and experiment. The investigation of the correlated bosons can be traced back to the study of ^{4}He.[2] Recently Jaksch has pointed out that the Bose-Hubbard model (BHM) Eq. (1) can well describe the ultracold boson atoms in an optical lattice, if one assumes a short-range pseudopotential interaction between the atoms and that the Wannier functions are well localized on the lattice site.[3,4]

The BHM has been studied using various analytical and numerical methods. In their seminal paper, Fisher *et al.*[5] used field theoretical approach to investigate the ground state of this model and obtained the superfluid (SF)-Mott insulator (MI) transition on the mean-field level. The Mott insulator is an incompressible state where integer number of bosons are localized on each site while the superfluid phase is compressible and has nonlocal boson wave functions. As an interesting phase, the ground state of MI is considered as a good candidate to realize the qubits for quantum information processing.[1,6,7] For weakly interacting bosons for which the fluctuations around the mean-field state are small, the Bogolubov theory or the Gross-Pitaevskii equation applies but both fail to predict the SF-MI transition.[8,9] Beyond the mean-field level, methods that can tackle the strong correlations have been applied,[3,5,9–12] including the Gutzwiller approach,[13,14] Bethe ansatz,[15] time-dependent variational principle method,[16] slave boson approach,[17–19] the strong-coupling expansion,[20–23] variational method based on mean-field theory,[24] variational cluster approach,[25] and the effective action approach,[24,26] etc. Recently the cavity method based on the Bethe lattice is also applied to BHM.[27] The numerical tools such as quantum Monte Carlo (QMC)[28–35] and density-matrix renormalization group[36,37] are used frequently for the unbiased studies.

The physics of the BHM depends critically on its spatial dimension. For a one-dimensional (1D) system, the Mermin-Wagner theorem[38] excludes the possibility of Bose-Einstein Condensation (BEC) at finite temperatures. In the strong-interaction regime, the bosons behave as the Tonks-Girardeau gas whose properties are similar to the noninteracting fermions.[4,39,40] The BEC in two dimensions (2D) can be viewed as a quasicondensate and the Mott transition is of the Kosterlitz-Thouless type.[4] The MI is strictly defined at zero temperature and the MI-BEC transition is a quantum transition well defined at zero temperature. However, there is a finite temperature range where the occupation is fixed at an integer. As temperature increases, the system changes from this Mott-type regime into the normal phase through a smooth crossover. For $D>2$, the SF phase also transits into the normal phase at a finite critical temperature.[28,41]

Experimentally, the BHM has been realized in the system of alkali-metal atoms in an optical lattice. The SF to MI transition has been observed in 1D, 2D, and three dimensional (3D), by changing the depth of the optical lattices.[42–44] These studies focused on the MI and the SF phase mainly in 2D and 3D (Refs. 41, 43, and 45–47) at finite temperatures. The temperature in these studies is a key factor and its effects on the observation cannot be ignored. Recent studies show that due to the finite temperature effects, the sharp peaks in the momentum distribution commonly adopted to identify the SF cannot be used as a reliable signature.[28,48,49] Due to technical difficulties, accurate studies for high-dimensional system ($D>2$) at finite temperatures that match the experiments are still highly desirable.

Here, we are interested in the strongly correlated bosons on a high-dimensional lattice ($D>2$) at finite temperatures, which received less attention in previous theoretical studies. One suitable method for our purpose is the dynamical mean-field theory (DMFT). DMFT is an exact theory in infinite spatial dimensions.[50] As an approximation for finite-dimensional systems, it has been widely used in the study of strongly correlated fermion systems and received much

success.[51] In a recent work, Byczuk and Vollhardt[52] extended the idea of DMFT to correlated boson systems and applied it to the bosonic Falicov-Kimball model. In their theory, instead of the usual way of scaling the hopping amplitude used in the fermionic DMFT, the contributions to the kinetic energy are separated into two parts, those from the condensate bosons and those from the normal bosons. Different scaling ansatz are used: scaling $t_{ij} \to \tilde{t}_{ij}/z^{|i-j|}$ for terms containing the anomalous averages $\langle b \rangle$ or $\langle b^\dagger \rangle$ and scaling $t_{ij} \to \tilde{t}_{ij}/\sqrt{z}^{|i-j|}$ for others. This guarantees that the energy density is finite as the spatial dimension goes to infinity, even if anomalous averages are involved in the boson systems. It should be noted that the derivation of the bosonic-DMFT (B-DMFT) equations is not unique. Recently, the essentially identical equations are also obtained by using an uniform scaling of $t \to \tilde{t}/z$ and keeping up to the subleading order in the $1/z$ expansion.[53] In this paper, we apply B-DMFT to the BHM. The resulting effective bosonic impurity model is solved by exact diagonalization (ED) method.[52,54] Results are presented for various phases at finite temperatures and compared to other theories and the experiments. The same method has been used in B-DMFT to study the single-component and two-component Bose-Hubbard model in Ref. 53.

This paper is organized as follows. In Sec. II, we briefly introduce the single band Bose-Hubbard model. We present the B-DMFT equations for the BHM, detail the impurity solver that we use, and give tests and benchmarks. In Sec. III, the main results of B-DMFT are shown and discussed. Section IV is a conclusion. We put some technical details in appendices.

II. MODEL AND METHOD

A. Bose-Hubbard model

The single band BHM is defined by the Hamiltonian below

$$H = -\sum_{\langle i,j \rangle} t_{ij} b_i^\dagger b_j + \frac{U}{2}\sum_i n_i(n_i-1) - \mu \sum_i n_i, \tag{1}$$

where $b_i^\dagger$ and b_i are the boson creation and annihilation operators on site i, respectively. They obey the commutation relation $[b_i, b_j^\dagger] = \delta_{i,j}$. $n_i = b_i^\dagger b_i$ is the boson number operator on the site i. Here, we consider the hopping amplitude $t_{ij} = t$ which is nonzero only for the nearest neighbors and U is the on-site energy. Feshbach resonances can be used to change the interaction strength over a wide range, even from repulsive to attractive.[4] In this paper we study the repulsive BHM with $U \geq 0$. We add the chemical potential μ which controls the number of bosons in the grand canonical ensemble. For simplicity, we take the density of states of the Bethe lattice, which is semicircular in the limit of infinite coordinations,

$$D(\epsilon) = \frac{1}{2\pi t^2}\sqrt{4t^2 - \epsilon^2}, \quad (|\epsilon| \leq 2t). \tag{2}$$

This density of states allows for an analytical calculation of the integral in the Dyson equation and is widely used in model studies using fermionic DMFT. For bosons, the low-energy behavior of density of states is important. Equation (2) has a $\sqrt{\epsilon}$ behavior near the band edge which is same as the 3D continuous boson systems.

B. B-DMFT equations

In DMFT, a lattice model is mapped into a single impurity problem with the self-consistently determined bath spectra. It becomes exact when the spatial dimension is infinite and hence ignores the spatial fluctuations from the outset. However, it fully takes into account the temporal fluctuations (imaginary time).[51] The key ingredient to extend the DMFT to bosons is a proper scaling of the hopping amplitude of bosons in the limit of infinite dimensions.[52]

We adopt the ansatz of scalings in Ref. 52 and implement similar derivations for the BHM. The detail of derivations can be found in Ref. 52. Here we present only the final B-DMFT equations. For simplicity, here we use the Nambu representation[55] for the boson operators $\mathbf{b}^\dagger(\tau) \equiv [b^\dagger(\tau) b(\tau)]$ and for the on-site interacting Green's functions (GFs) as in Ref. 52

$$\begin{aligned}\mathbf{G}(\tau-\tau') &\equiv -\langle T_\tau[\mathbf{b}(\tau)\mathbf{b}^\dagger(\tau')]\rangle \\ &= \begin{pmatrix} -\langle T_\tau[b(\tau)b^\dagger(\tau')]\rangle & -\langle T_\tau[b(\tau)b(\tau')]\rangle \\ -\langle T_\tau[b^\dagger(\tau)b^\dagger(\tau')]\rangle & -\langle T_\tau[b^\dagger(\tau)b(\tau')]\rangle \end{pmatrix} \\ &= \begin{pmatrix} G_1(\tau-\tau') & G_2(\tau-\tau') \\ G_3(\tau-\tau') & G_4(\tau-\tau') \end{pmatrix}. \end{aligned} \tag{3}$$

According to the definition, the following relations hold for the components $G_3(\tau-\tau') = G_2^*(\tau-\tau')$ and $G_4(\tau-\tau') = G_1^*(\tau-\tau')$.

The action for the effective impurity model obtained through the cavity method[51] reads

$$\begin{aligned} S_{eff} = &\int_0^\beta d\tau \int_0^\beta d\tau' \mathbf{b}_0^\dagger(\tau)[-\mathcal{G}_0^{-1}(\tau-\tau')]\mathbf{b}_0(\tau') \\ &+ \int_0^\beta d\tau \frac{U}{2} n_0(\tau)[n_0(\tau)-1] + \int_0^\beta d\tau \mathbf{\Phi}_0^\dagger \mathbf{b}_0(\tau). \end{aligned} \tag{4}$$

In this equation, $\mathbf{\Phi}_0$ is related to the condensation via

$$\mathbf{\Phi}_0^\dagger = (-\tilde{t}\langle b_0^\dagger \rangle_{S_{eff}} - \tilde{t}\langle b_0 \rangle_{S_{eff}}). \tag{5}$$

Here $\tilde{t}$ is the hopping amplitude after the scaling has been carried out. $\langle b_0^\dagger \rangle$ is treated as a τ-independent quantity since we are studying an equilibrium theory. The Weiss field $\mathcal{G}_0^{-1}(i\omega_n)$ represents the effective field from the environmental fluctuations acting on the impurity site.

The self energy is defined through the Dyson equation

$$\mathbf{\Sigma}(i\omega_n) = 2\mathcal{G}_0^{-1}(i\omega_n) - \mathbf{G}_c^{-1}(i\omega_n). \tag{6}$$

Here, $\mathbf{G}_c$ is the connected GF defined as

$$\mathbf{G}_c(\tau-\tau') = \mathbf{G}(\tau-\tau') - \mathbf{G}_{dis}(\tau-\tau'), \tag{7}$$

where $\mathbf{G}_{dis}(\tau-\tau')$ is the disconnected part. Its Fourier transform is given in Appendix C. In the imaginary time axis it is a constant and coincides with the condensed fraction in the thermal dynamical limit. $\mathbf{\Sigma}$ and $\mathcal{G}_0$ have the same symmetry

properties as the GF. Among the four matrix elements only two functions are independent. It is noted that the definition of the self-energy in Eq. (6) has a factor of 2 difference from Eq. (11) in Ref. 52. This difference can be traced back to the different conventions used for path integrals in Nambu representation.[56] We have checked that our equations are self-consistent and they guarantee $\mathbf{\Sigma}(i\omega_n)=0$ for $U=0$.

The connected local GF of the lattice Hamiltonian is given by the lattice Dyson equation

$$\mathbf{G}_c(i\omega_n) = \frac{1}{N_{latt}} \sum_k \{[\mathbf{G}_c^{(0)}]^{-1}(k,i\omega_n) - \mathbf{\Sigma}(i\omega_n)\}^{-1}. \quad (8)$$

Here N_{latt} is the total lattice number. $\mathbf{G}_c^{(0)}(k,i\omega_n)$ is the connected GF of the noninteracting system $H_0=\Sigma_k(\epsilon_k-\mu)b_k^\dagger b_k$. It reads

$$\mathbf{G}_c^{(0)}(k,i\omega_n) = [i\omega_n\sigma_3 - (\epsilon_k-\mu)\mathbf{I}]^{-1}. \quad (9)$$

In the actual calculations, we transform the summation over k in Eq. (8) into the integral over energy. The explicit integral formulas involving the semicircular density of states, Eq. (A2), are summarized in Appendix A. Equations (3)–(9) constitute the B-DMFT self-consistency equations for the BHM.

C. Impurity solver

In order to solve the B-DMFT equations, a suitable impurity solver should be selected. To avoid technical complexities we use the exact diagonalization method to solve the impurity model. It is simple, fast, while at the same time qualitatively keeps the nontrivial many-body physics of the problem.[57] The effective impurity Hamiltonian equivalent to the action Eq. (4) reads

$$H_{imp} = \sum_{k=1}^{B_s} \mathbf{a}_k^\dagger \mathbf{E}_k \mathbf{a}_k + \sum_{k=1}^{B_s} (\mathbf{a}_k^\dagger \mathbf{V}_k \mathbf{b}_0 + \mathbf{b}_0^\dagger \mathbf{V}_k^\dagger \mathbf{a}_k) + \frac{U}{2} n_0(n_0-1) + \mathbf{\Phi}_0^\dagger \mathbf{b}_0. \quad (10)$$

The creation and annihilation operators $\mathbf{a}_k^\dagger$ and $\mathbf{a}_k$ are for the environmental degrees of freedom and are all in the Nambu representation. B_s is the number of bath sites. $\mathbf{E}_k$ and $\mathbf{V}_k$ are the kinetic energy of environmental bosons and the coupling strength between the environment and the impurity, respectively. They are 2×2 matrices, $\mathbf{E}_k=\begin{pmatrix} E_{k1} & E_{k2} \\ E_{k3} & E_{k4} \end{pmatrix}$ and $\mathbf{V}_k=\begin{pmatrix} V_{k1} & V_{k2} \\ V_{k3} & V_{k4} \end{pmatrix}$. From the Hermiticity of $H_{imp}=H_{imp}^\dagger$, we have $E_{k4}=E_{k1}$ being real, $E_{k3}=E_{k2}^*$, $V_{k3}=V_{k2}^*$, and $V_{k4}=V_{k1}^*$. The requirement that H_{imp} is equivalent to the effective action S_{eff} in Eq. (4) gives the following relation (see Appendix B) between $\mathcal{G}_0^{-1}$ and $\mathbf{E}_k$, $\mathbf{V}_k$,

$$\mathcal{G}_0^{-1}(i\omega_n) = \left[\frac{1}{2} i\omega_n \sigma_3 + \frac{1}{2}\mu\mathbf{I} - \sum_{k=1}^{B_s} \mathbf{V}_k \left(\frac{1}{2} i\omega_n \sigma_3 - \mathbf{E}_k \right)^{-1} \mathbf{V}_k^\dagger \right]. \quad (11)$$

We solve the B-DMFT equations using an iterative scheme as usually done for fermions. We start from an initialization of the parameters $\mathbf{E}_k$, $\mathbf{V}_k$ $(k=1,..,B_s)$ and $\mathbf{\Phi}_0$. With them we calculate $\mathcal{G}_0^{-1}(i\omega_n)$ and define the impurity model Eq. (10). The impurity Hamiltonian is then solved by ED to produce the connected GF $\mathbf{G}_c$ and a new $\mathbf{\Phi}_0$, according to the following equation:

$$\mathbf{G}_c(i\omega_n) = \mathbf{G}(i\omega_n) - \mathbf{G}_{dis}(i\omega_n) \quad (12)$$

and

$$\mathbf{\Phi}_0 = -\tilde{t}\langle \mathbf{b}_0 \rangle. \quad (13)$$

Here $\langle \cdots \rangle$ represents the average under H_{imp}. $\mathbf{G}$ is calculated from the Lehmann representation. $\mathbf{G}_{dis}(i\omega_n)$ is the disconnected Green's function. Details are in Appendix C.

Using Eq. (6), one obtains the self-energy $\mathbf{\Sigma}$ from $\mathbf{G}_c$. It is then put into the lattice Dyson equation Eq. (8) to produce a new $\mathbf{G}_c$. Using Eq. (6) again, we update the Weiss field $\mathcal{G}_0$ and from it we get the new parameters $\mathbf{E}_k$ and $\mathbf{V}_k$ through the following fitting procedure.[51] A distance function $D[\mathbf{E}_k,\mathbf{V}_k]$ is defined as

$$D[\mathbf{E}_k,\mathbf{V}_k] = \sum_n [|\mathcal{G}_{01}^{-1}(i\omega_n) - \tilde{\mathcal{G}}_{01}^{-1}(i\omega_n)| + |\mathcal{G}_{02}^{-1}(i\omega_n) - \tilde{\mathcal{G}}_{02}^{-1}(i\omega_n)|]. \quad (14)$$

Here $\tilde{\mathcal{G}}_0^{-1}$ is calculated from $\mathbf{E}_k$ and $\mathbf{V}_k$ through Eq. (11). $D[\mathbf{E}_k,\mathbf{V}_k]$ is then minimized with respect to $\mathbf{E}_k$ and $\mathbf{V}_k$ to find the optimal parameters that can reproduce $\mathcal{G}_0^{-1}(i\omega_n)$ best. With these optimal parameters we define an impurity model to be diagonalized again. The iteration continues until the lattice GF converges.

One specialty of boson is that it has an infinitely large local Hilbert space. This poses difficulty for ED-based numerical methods when adapted for bosons.[58] In our ED calculations, we truncate the local Hilbert space by using $N+1$ boson states for each mode, with N a finite number. As the simplest algorithm, we use the boson number eigen state $|n\rangle(n=0,1,\ldots,N)$ as our local basis and keep the implementation of optimal basis for a future improvement.[59] The truncation of boson Hilbert space introduces additional approximation and influences the accuracy of our results, especially in the BEC phase (see below). It is therefore important to check our results with respect to N and to make sure that the truncation errors are under control.

However, the truncation described above introduces a new problem to the commutation relation of boson operators. In the truncated Hilbert space, one has

$$b = \begin{pmatrix} 0 & 1 & 0 & \cdots & 0 & 0 \\ 0 & 0 & \sqrt{2} & \cdots & 0 & 0 \\ 0 & 0 & 0 & \cdots & 0 & 0 \\ \vdots & \vdots & \vdots & \cdots & \vdots & \vdots \\ 0 & 0 & 0 & \cdots & 0 & \sqrt{N} \\ 0 & 0 & 0 & \cdots & 0 & 0 \end{pmatrix} \quad (15)$$

and $b^\dagger$ is the Hermitian conjugate matrix of b. From these one gets $bb^\dagger=\mathrm{diag}\{1,2,\ldots,N,0\}$ and $b^\dagger b=\mathrm{diag}\{0,1,\ldots,N-1,N\}$. The commutation relation reads $[b,b^\dagger]=\mathrm{diag}\{1,1,\ldots,-N\}$ with the incorrect trace $\mathrm{Tr}[b,b^\dagger]=0$.

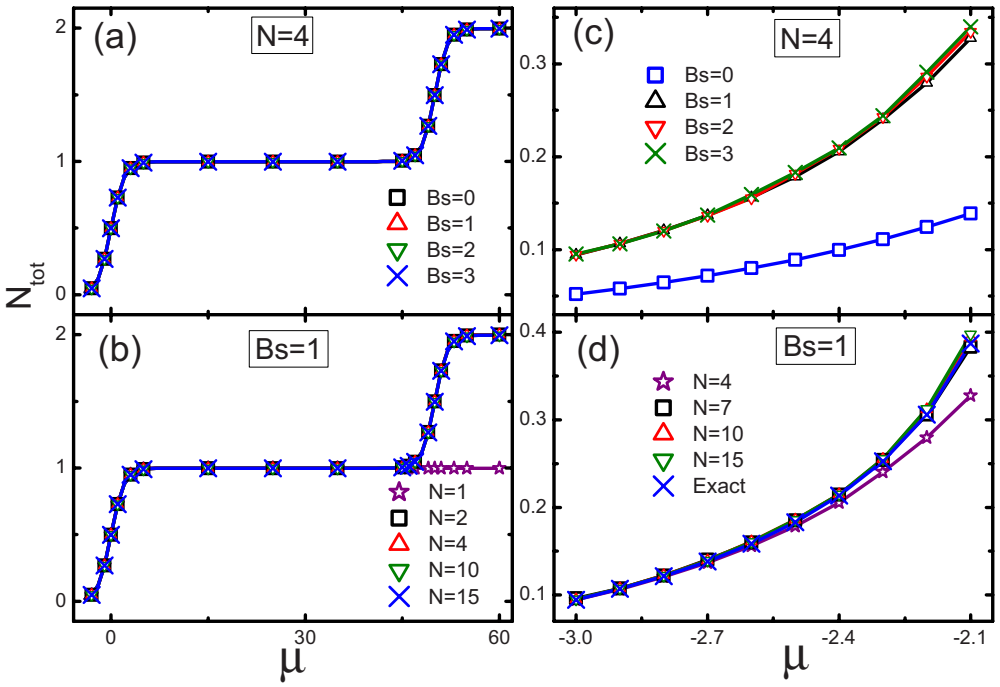

FIG. 1. (Color online) The total boson occupation as functions of chemical potential μ. [(a) and (b)]: $U=50.0$, $\tilde{t}=0$, and $T=1.0$; (c) and (d): $U=0$, $\tilde{t}=1.0$, and $T=1.0$.

Therefore, using representation Eq. (15) in our calculation will lead to incorrect weight in the GFs as well as in the density of states. This problem cannot be remedied by increasing N. To overcome this difficulty, we modify the representation of b ($b^\dagger$ accordingly) into

$$b=\begin{pmatrix} 0 & 1 & 0 & \cdots & 0 & 0 \\ 0 & 0 & \sqrt{2} & \cdots & 0 & 0 \\ 0 & 0 & 0 & \cdots & 0 & 0 \\ \vdots & \vdots & \vdots & \cdots & \vdots & \vdots \\ 0 & 0 & 0 & \cdots & 0 & \sqrt{N} \\ 0 & 0 & 0 & \cdots & 0 & \sqrt{N+1} \end{pmatrix}. \tag{16}$$

It produces $b^\dagger b=\mathrm{diag}\{0,1,\ldots,N-1,2N+1\}$, $[bb^\dagger]_{i,i}=i(i=1,\ldots,N+1)$, and $[bb^\dagger]_{N,N+1}=[bb^\dagger]_{N+1,N}=\sqrt{N(N+1)}$. The trace $\mathrm{Tr}[b,b^\dagger]=0$ is still incorrect. However, $b^\dagger b$ from representation Eq. (15) and $bb^\dagger$ from Eq. (16), if combined together, give the correct trace $\mathrm{Tr}[b,b^\dagger]=N+1$ Therefore, our strategy is that for any operators involving $b^\dagger b$, such as $\langle i|b^\dagger|j\rangle\langle j|b|i\rangle$ in the Lehmann representation of the diagonal GF, we use Eq. (15). For operators involving $bb^\dagger$ such as $\langle i|b|j\rangle\langle j|b^\dagger|i\rangle$, we use Eq. (16) [see Eqs. (C2) and (C3) in Appendix C]. In this way, the truncation introduced boson commutation problem is solved.

For the bosonic impurity model Eq. (10) with B_s bath sites and $N+1$ states for each boson mode, the dimension of the Hilbert space is $S_t=(N+1)^{B_s+1}$. To describe the BEC phase where $\mathbf{\Phi}_0\neq 0$, the total particle number can no longer be used as a good quantum number. In this case both ED and calculating the GFs are very time consuming. As a result, the parameters N and B_s are severely limited by the present computer power. In the DMFT (ED) study of the Fermi Hubbard model with four states on each site, it was shown that results converge quite fast with the bath site number B_s and $B_s=4$ already gives qualitatively reliable results.[51] To explore the B_s and N dependence of calculations for the Bose-Hubbard model, we calculate the N_{tot}-μ curves in both the atomic and the free boson limit for different N and B_s values. The results are shown in Fig. 1. In both limits, as long as the bath site number B_s is larger than zero, the results are already very close to the exact ones. At the same time, N dependence is more severe. The curves keep improving observably until $N\geq 10$. Taking a compromise between N and B_s, in our study we do all the calculations at $B_s=1$ (one bath site) and $N=15$ (16 boson states) unless stated otherwise. We check our results using larger N and B_s and make sure that our conclusion does not depend on the selection of B_s and N. For the Matsubara frequencies $\omega_n=2n\pi/\beta$ in the GFs, we use the cut off $|\omega_n|\leq 2000$.

D. Noninteracting limit and atomic limit

In this section, we check the B-DMFT formulas and our numerical results in the noninteracting as well as in the atomic limit. For a noninteracting boson system, the bosons can move freely in the lattices. They condense into a single-particle state when the temperature is lower than T_c. The exact solution of the Bose-Hubbard model in this limit gives the thermally excited boson occupation N_e as

$$N_e=\int_{-\infty}^{\infty} d\epsilon \frac{D(\epsilon)}{e^{\beta(\epsilon-\mu)}-1}. \tag{17}$$

The B-DMFT equations [Eqs. (3)–(9)] can also be solved exactly in this limit.[52] At $U=0$, by carrying out the Gaussian

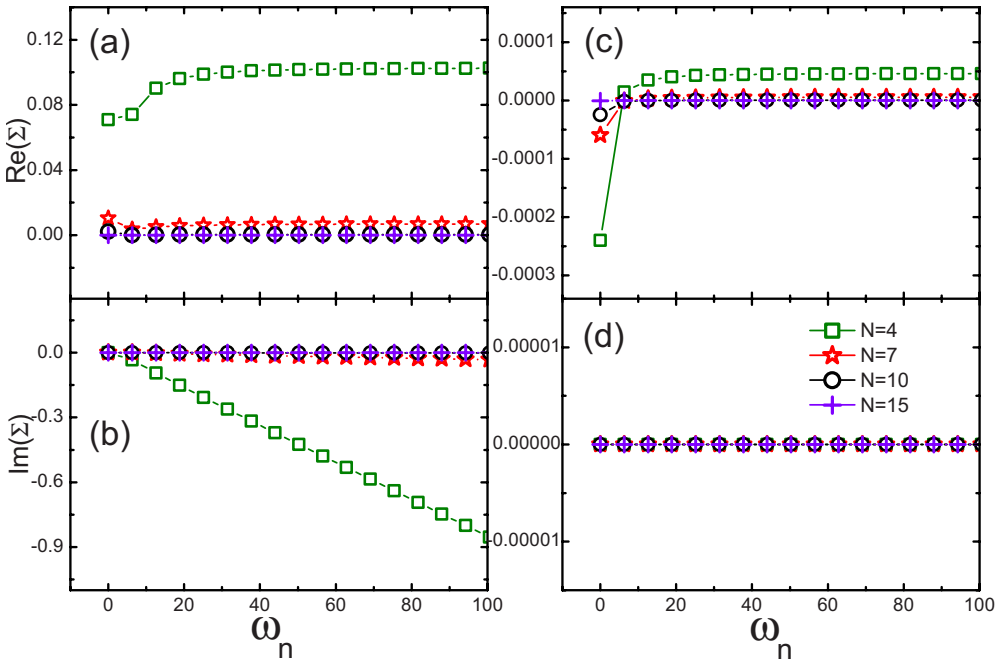

FIG. 2. (Color online) The self-energy of the noninteracting system as a function of Matsubara frequency. [(a) and (b)]: diagonal component $\mathbf{\Sigma}_1$; (c) and (d): off-diagonal component $\mathbf{\Sigma}_2$. They are calculated at $U=0$, $\tilde{t}=1.0$, $\mu=-2.1$, and $T=1.0$. Symbols are denoted in the figure.

integral in Eq. (4) and doing the functional derivative of the free energy with respect to $\mathcal{G}_0^{-1}$ (subtracting the disconnected contribution), we get the connected GF as

$$\mathbf{G}_c(i\omega_n) = \frac{1}{2}\mathcal{G}_0(i\omega_n), \tag{18}$$

which is independent of $\mathbf{\Phi}_0$. This gives a zero self-energy $\mathbf{\Sigma}(i\omega_n)=0$ according to Eq. (6), as expected. From Eqs. (8) and (9) we obtain the GF

$$\mathbf{G}_c(i\omega_n) = \int_{-\infty}^{\infty} d\epsilon D(\epsilon)[i\omega_n\sigma_3 - (\epsilon-\mu)\mathbf{I}]^{-1}. \tag{19}$$

It is the exact result for the free bosons. The expression (17) for the thermal excited particle number N_e can be recovered from it using the fluctuation-dissipation theorem.

The order parameter of BEC reads

$$\langle \mathbf{b}_0^\dagger \rangle = \frac{1}{Z}\int \mathcal{D}b_0^* \mathcal{D}b_0 \mathbf{b}_0^\dagger \exp(-S_{eff}) = \frac{1}{2}\mathbf{\Phi}_0^\dagger \mathcal{G}_0(i0). \tag{20}$$

Together with Eq. (5), it gives

$$\mathbf{\Phi}_0^\dagger \begin{cases} =0, & \mu < -2\tilde{t}, \text{ for normal phase,} \\ \neq 0, & \mu = -2\tilde{t}, \text{ for BEC phase.} \end{cases} \tag{21}$$

Considering that for $\mu=-2\tilde{t}$, $\mathbf{G}_c(i0)=-(1/\tilde{t})\mathbf{I}$, we cannot determine the nonzero value of $\mathbf{\Phi}_0$ in the BEC phase solely from the self-consistency equations. This corresponds to the fact that for free bosons, the condensed fraction cannot be fixed without giving the total particle number N_{tot}. The results above can also be obtained from the equation of motion of GFs, starting from the impurity Hamiltonian (10) with $U=0$. From this approach one gets

$$\mathbf{G}_c(i\omega_n) = \left[i\omega_n\sigma_3 + \mu\mathbf{I} - 4\sum_k \mathbf{V}_k(i\omega_n\sigma_3 - 2\mathbf{E}_k)^{-1}\mathbf{V}_k^\dagger \right]^{-1} \tag{22}$$

and

$$\langle \mathbf{b}_0^\dagger \rangle = \mathbf{\Phi}_0^\dagger \left[\mu\mathbf{I} + 2\sum_k \mathbf{V}_k\mathbf{E}_k^{-1}\mathbf{V}_k^\dagger \right]^{-1}. \tag{23}$$

Substituting the parameters $\mathbf{E}_k$ and $\mathbf{V}_k$ with the $\mathcal{G}_0$ in Eq. (11), we can get the same results as Eqs. (18) and (20).

In Fig. 2, the real and imaginary parts of the self-energy are shown for $U=0$. Both the diagonal and off-diagonal components tend to zero as the number of boson states N increases. The self-energy is not strictly zero for finite N because in the truncated space, boson operators do not obey canonical commutation relations and even $U=0$ does not correspond to a free system. From Fig. 3, it is seen that the $N_e-\mu$ curves from B-DMFT at $U=0$ agree well with the exact ones. The deviation at high temperatures decreases as N increases, consistent with what we find in Fig. 2.

In the atomic limit $\tilde{t}=0$, the quantum fluctuations of the boson number operators disappear. Each site has an integer number of localized particles at zero temperature. As the temperature increases, thermal fluctuations dominate and the localized state will melt gradually. In this limit, $\mathbf{\Phi}_0=0$ according to Eq. (5). The density of states $D(\epsilon)$ becomes a delta function and Eq. (8) reduces to

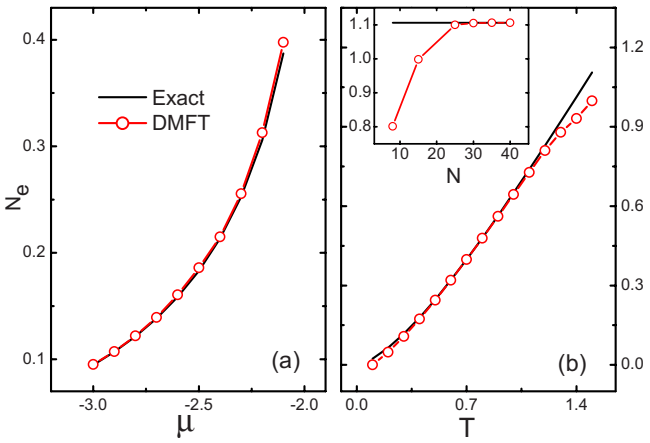

FIG. 3. (Color online) DMFT result (dots with eye-guiding lines) and the exact result (solid line) for the thermal excited boson number N_e at $U=0$ and $\tilde{t}=1.0$. (a) as a function of μ at $T=1.0$; (b) as a function of T at $\mu=-2\tilde{t}$. Inset: N_e as a function of N at $\mu=-2\tilde{t}$ and $T=1.5$.

$$\mathbf{G}_c(i\omega_n)=[i\omega_n\sigma_3+\mu\mathbf{I}-\mathbf{\Sigma}(i\omega_n)]^{-1}. \tag{24}$$

Comparing with Eq. (6), one gets $\mathcal{G}_0^{-1}(i\omega_n)=(i\omega_n\sigma_3+\mu\mathbf{I})/2$. When inserted into the effective action Eq. (4), it gives exactly the action in the atomic limit. Our numerical results for the atomic limit obtained using $B_s=1$ and $N=15$ are shown in Fig. 4. The B-DMFT results (squares with guiding lines) agree well with the exact ones (curves). Note that in the atomic limit, the B-DMFT results depend very weakly on B_s and N. It is seen that the thermal activation will smear the Mott plateaus and the compressibility $\partial N_{tot}/\partial\mu$ has broadened peaks. For $U=50$, the Mott plateaus are clear at low temperatures and their features disappear completely at about $T=10$. This observation agrees with the conclusion that the MI melts completely at about $T^*=0.2U$ in the limit $\tilde{t}=0$.[41]

III. RESULTS AND DISCUSSIONS

In this section we discuss the physical results obtained by the B-DMFT for the BHM. At zero temperature, the system should be either in the BEC phase for weak interaction or in the MI phase for strong interaction. At finite temperatures, besides the BEC and MI phases that are extended from the ground state, there is the normal phase that is connected to the MI and BEC phases in low-temperature regimes, through a crossover and a second-order phase transition, respectively. Figures 5(a) and 5(b) show the diagonal component of the converged connected GFs typical for the BEC, MI, and normal phases. They are calculated at a finite but low temperature $T/U=0.05$. All the high-energy parts show the expected behavior $\mathrm{Re}\,G_{c1}(i\omega_n)\propto 1/\omega_n^2$ and $\mathrm{Im}\,G_{c1}(i\omega_n)\propto 1/\omega_n$. The low-energy behaviors are markedly different between the MI phase and the other two. Similar to the MI phase of fermions, $\mathrm{Im}\,G_{c1}(i\omega_n)\to 0$ at zero frequency, signaling strong scattering and nonexistence of well-defined low-energy quasiparticles in the MI phase. In contrast, in the BEC and the normal phases, the diagonal connected GFs are qualitatively similar. In Figs. 5(c) and 5(d) are the corresponding off-diagonal GFs in the three phases. The condensation in the BEC phase contributes to a sharp peak in the low-energy regime of Re G_{c2}. While in the MI and the normal phases, no such peak appears. In all the three phases, Im $G_{c2}=0$ as it is required by its definition and symmetry.

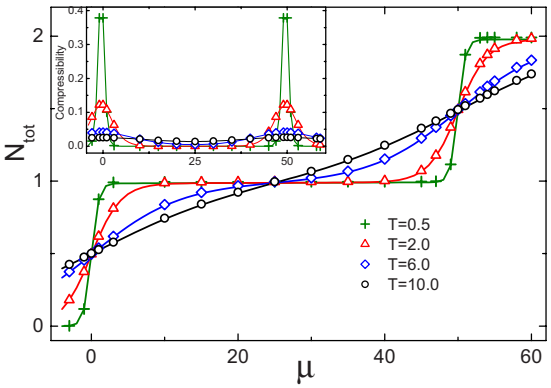

FIG. 4. (Color online) The total number of bosons as functions of the chemical potential μ in the atomic limit with $U=50.0$ for different temperatures. The lines are the exact results and symbols for B-DMFT results. Inset: the compressibility $\partial N_{tot}/\partial\mu$ as functions of μ obtained from B-DMFT.

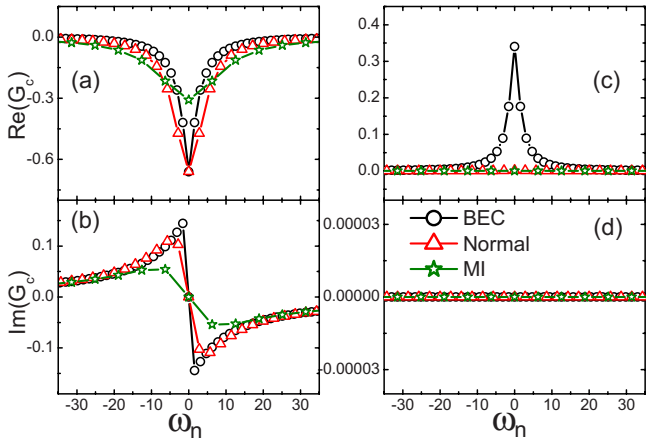

FIG. 5. (Color online) [(a) and (b)] The connected diagonal GF G_{c1} and [(c) and (d)] off-diagonal GF G_{c2} in the three phases: BEC phase (circle): $\tilde{t}/U=0.2$; normal phase (triangle): $\tilde{t}/U=0.11$; and MI phase (pentacle): $\tilde{t}/U=0.05$. All are calculated at $\tilde{t}=1.0$, $\mu/U=0.5$, and $T/U=0.05$.

The full GF (not shown in Fig. 5) can be written as the form $G_m(i\omega_n)=G_{cm}(i\omega_n)+\Delta_m\delta_{n,0}$, $(m=1,2)$. For the BEC phase shown in Fig. 5, our numerical calculation gives $\Delta_1=-2.72$, $\Delta_2=-2.71$, and $-\beta\langle b_0\rangle^2=-2.61$. Within numerical errors, our result is consistent with the equation $\Delta_1=\Delta_2=-\beta\langle b_0\rangle^2$ as can be seen from the Lehmann expressions for GF in Appendix C. For the MI and the normal phases, we always get $\Delta_1=\Delta_2=0$.

The total particle occupation is calculated by

$$N_{tot}=-\frac{1}{\beta}\sum_n G_{c1}(i\omega_n)e^{i\omega_n 0^+}+\langle b_0\rangle^2, \tag{25}$$

where the condensed boson number N_0 is

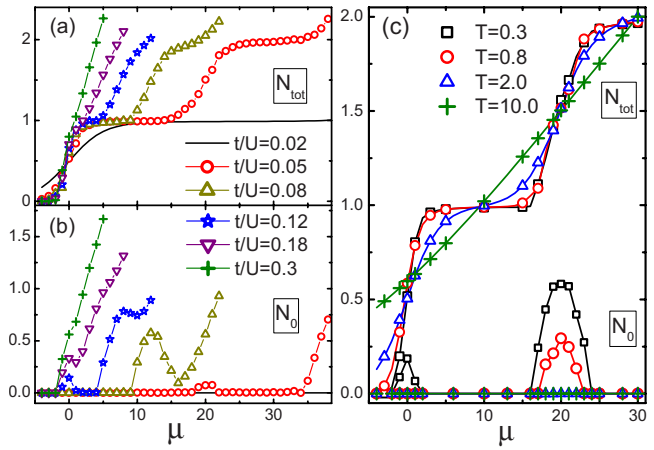

FIG. 6. (Color online) N_{tot} and N_0 as functions of μ. [(a) and (b)] $T/U=0.05$ for different $\tilde{t}/U$ ($\tilde{t}=1.0$); (c) $\tilde{t}=1.0$, $\tilde{t}/U=0.05$ for different temperatures. Symbols with eye-guiding lines are denoted in the figure.

$$N_0 = \langle b_0 \rangle^2. \tag{26}$$

For $U>0$, a simple mean-field analysis shows that the free energy becomes a quartic function for large $\langle b_0 \rangle$ and hence both N_0 and N_{tot} can be determined solely by the B-DMFT equations. They are plotted in Fig. 6 as functions of the chemical potential. In Fig. 6(a) we fix $T/U=0.05$ and study the evolution of the curves as $\tilde{t}/U$ decreases. For large $\tilde{t}/U$ (small U for fixed $\tilde{t}$), N_{tot} and N_0 are increasing functions of μ up to a boundary of μ and the system always stay in the BEC phase. At the boundary, the convergence becomes slow and difficult. As $\tilde{t}/U$ is smaller, a plateau of $N_{tot}=1$ begins to emerge in the N_{tot}-μ curve. N_0 has a temporal decreases at the corresponding μ and then continues to increase. The system is still in BEC phase but the plateau and the dip in N_0 show the precursor to the MI phase. As $\tilde{t}/U$ still decreases, the plateau enlarges at $N_{tot}=1$ and the next one at $N_{tot}=2$ begins to appear, forming Mott-type regimes. N_0 has a well-formed gap corresponding to each plateau and has a peak signaling BEC between two neighboring gaps. These BEC phases appear around $\mu=0,U,2U,\ldots$ where two adjacent Mott plateaus are connected. As $\tilde{t}/U$ decreases, the height of the N_0 peak decreases and the critical temperature T_c also decreases [see Fig. 8(b)]. For very large U such as $\tilde{t}/U=0.02$, BEC does not appear any more because the critical temperature is lower than the actual T, $(T/U)_c < T/U=0.05$ at $\tilde{t}/U=0.02$. Figure 6(c) shows the temperature evolution at a fixed $\tilde{t}/U=0.05$. The temperature effects on the Mott plateau as well as on the BEC phase are clearly observable. As temperature rises, the Mott plateaus gradually blur at the shoulders and the condensed boson number N_0 reduces to zero. For high enough temperature, the Mott plateaus finally disappear and the MI crosses over to the normal phase.

A recent B-DMFT study for the bosonic Falicov-Kimball model reveals that the local repulsion enhances the transition temperature of BEC.[52] Here we study the influence of U on BEC in the BHM. In Fig. 7, we plot the N_0-T curves at different $\tilde{t}/U$ values for a fixed total density $N_{tot}=1.5$. For a

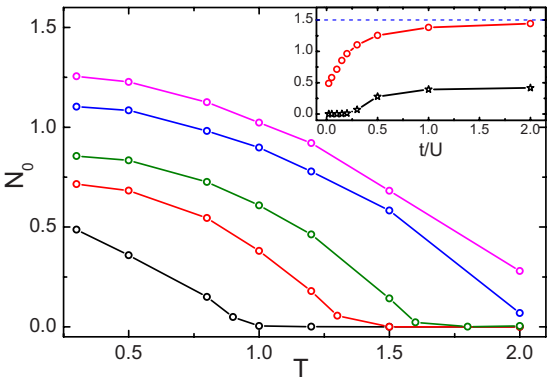

FIG. 7. (Color online) The condensed boson number N_0 as functions of temperature T for fixed total number $N_{tot}=1.5$ and different $\tilde{t}/U$ ($\tilde{t}=1.0$). From top to bottom, $\tilde{t}/U=0.5,0.3,0.15,0.1,0.02$, respectively. Inset: N_0 changes with $\tilde{t}/U$ for $T=0.3$ (circle) and $T=2.0$ (pentacle), respectively. The dashed line is $N_0=1.5$. Solid lines are guiding lines.

given $\tilde{t}/U$, N_0 is a decreasing function of T and reduces to zero at T_c. With decreasing $\tilde{t}/U$ values (increasing $U/\tilde{t}$), the N_0-T curve shifts downward, leading to smaller N_0 for a given T and a reduction in T_c. This is consistent with the naive picture that strong local repulsion between bosons tends to suppress the particle number fluctuations and act against the BEC. Also, the quasiparticle states into which the bosons can condense are turned into incoherent states and shifted into the Hubbard bands by a large U. Therefore, our conclusion is that, different from the bosonic Falicov-Kimball model, the local repulsion in the BHM reduces the transition temperature of BEC.

Different phases in the system can be distinguished from N_{tot} and N_0. At zero temperature, the system has two phases: the BEC phase and the MI phase. Due to the competition between the on-site repulsion U and the hopping t, there is a quantum phase transition between them. As temperature increases, the BEC phase and the MI phase will change into normal phase through a phase transition and a crossover, respectively. We have therefore three phases to identify at finite temperatures: a nonzero N_0 signals the BEC phase while the MI has $N_0=0$ and an integer N_{tot} with zero compressibility $\partial N_{tot}/\partial\mu$; the phase with $N_0=0$ but a finite compressibility is the normal phase. According to this criterion, we plot the phase diagrams in Fig. 8.

In Fig. 8(a) is the phase diagram on the μ/U-$\tilde{t}/U$ plane for finite temperature $T/U=0.05$. It is obtained by scanning μ/U at fixed $\tilde{t}/U$. Three regimes are clearly shown, the MI phase, the BEC phase, and the normal phase. Due to the small N parameter that we use, only the $N_{tot}=1$ and part of the $N_{tot}=2$ MI domains are obtained. In the large $\tilde{t}/U$ regime, BEC is stable. Between the two boundaries (circles and pentacles) is the normal phase. The melting temperature T^* and BEC transition temperature T_c are marked by pentacles and circles, respectively. Similar finite temperature phase diagram is also obtainable from a static mean-field theory.[12] To understand the temperature effects on this diagram, we resort to phase diagrams on the T/U-$\tilde{t}/U$ plane at two different μ/U values, Figs. 8(b) and 8(c). At $T=0$, a BEC-MI quan-

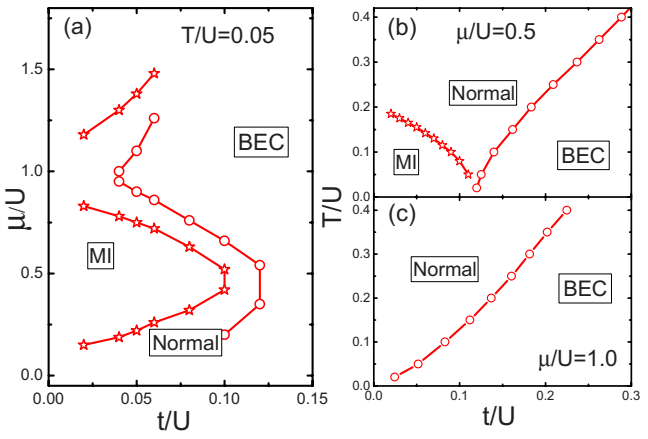

FIG. 8. (Color online) Phase diagrams. (a) in μ/U-$\tilde{t}/U$ plane at $T/U=0.05$; (b) and (c) in T/U-$\tilde{t}/U$ plane at $\mu/U=0.5$ and $\mu/U=1.0$, respectively. Three phases, the BEC, normal, and MI phases are marked out in the figures. Lines are for eye guiding.

tum phase transition occurs at a critical $\tilde{t}/U$. The difference between Figs. 8(b) and 8(c) shows that $(\tilde{t}/U)_c$ is dependent on μ/U, consistent with the lobe shape of the MI boundary in Fig. 8(a). At finite temperatures, the normal phase appears as a quantum critical regime extending from the $T=0$ quantum critical point. This hints that in the normal phase near $(\tilde{t}/U)_c$, critical behavior such as power-law correlation should exist. Experimental observation of such quantum critical features in the normal phase near $(t/U)_c$ will be an interesting issue.

A representative quantity for comparison between different theories is the critical value $(t/U)_c$ at the tip of the $n=1$ Mott lobe. It has been obtained by various methods. For the 3D cubic lattice, the world line QMC gives $(t/U)_c=0.032$ (Ref. 28) and the worm algorithm QMC gives $(t/U)_c=0.03408$ (Ref. 34). Recent studies for the Bethe lattice with $z=6$ give $(t/U)_c=0.033$ (Ref. 27) and $(t/U)_c=0.032$ (Ref. 53). In our study, we obtained $(\tilde{t}/U)_c=0.12$ for $\mu/U=0.5$ ($n=1$ Mott lobe). The apparent discrepancy between our value and the previous ones is because we did not use the realistic lattice structure. In our calculations, we take $z=\infty$ literally and set $\tilde{t}=1$ as the energy unit, hence z does not appear explicitly. Since different scalings relating $\tilde{t}$ to t are used in B-DMFT for the normal and the condensed bosons, a critical value for $z=6$ cannot be simply recovered from our result by doing an inverse scaling. A crude estimation, however, gives $(t/U)_c \approx 0.12/z \sim 0.12/\sqrt{z}=0.02 \sim 0.049$ for $z=6$, being consistent with the more accurate values.

For realistic lattices with a finite coordinate z, the B-DMFT is still applicable but should be regarded as an approximation to finite-dimensional systems. For such a calculation, one should use the actual dispersion ϵ_k of the given lattice in Eq. (9) and replace $\tilde{t}$ with zt in Eq. (5). Experimentally, the BEC-MI transition point was observed for ^{87}Rb atoms in 3D optical lattices.[42] The transition occurs at a potential depth of $13E_r$ which compares favorably with the mean-field value $U/t=5.8z$ (Refs. 9, 10, and 12) but differs from the more accurate QMC results cited above. The B-DMFT calculation for the BHM in 3D cubic lattice and quantitative comparison with the experiments as well as with the previous theoretical results will be an interesting topic. But this is only attainable when an accurate impurity solver is available. Therefore we leave it for future study.

Finally we note that the ED method used in this work poses limitations to our study. Due to finite number of boson states $N=15$, reliable calculations are only possible in the small N_{tot} and small N_0 regimes. The small number of bath sites $B_s=1$ causes slow convergence, especially near the MI-BEC transition. Therefore, for practical applications of B-DMFT to boson systems, it is necessary to develop an accurate and fast impurity solver. In this respect, the recently developed bosonic NRG is a promising technique.[54,58] For the ED method, an algorithm adopting the optimal boson basis will be interesting and progress is being made in this direction.

IV. CONCLUSION

In this paper we have performed the B-DMFT study for the BHM. Following the ansatz of scaling in Ref. 52, we obtain the B-DMFT equations for the BHM. The bosonic effective impurity Hamiltonian is solved by ED method with truncated boson Hilbert space. We focus on the finite temperature properties of the correlated bosons and identify the MI, BEC, and the normal phases. The repulsive U is found to suppress the BEC transition temperature T_c. Phase diagrams on the μ/U-$\tilde{t}/U$ and T/U-$\tilde{t}/U$ planes are obtained, which disclose the quantum critical nature of the low-temperature normal phase. Relevance of our results to other theoretical ones and the experimental observations are discussed.

ACKNOWLEDGMENTS

We thank Krzysztof Byczuk and Dieter Vollhardt for helpful discussions and their comments on the manuscript. We also thank Anna Kauch for pointing our error in our formula. This work is supported by NSFC under Grant No. 10674178 and the 973 Program of China (Grant No. 2007CB925004).

APPENDIX A: INTEGRAL OF SEMICIRCULAR DENSITY OF STATES

The lattice Dyson equation in the B-DMFT equations [Eq. (8)] is usually transformed into an integral over ϵ of the form

$$\mathbf{G}_c(i\omega_n) = \int d\epsilon D(\epsilon)[i\omega_n\sigma_3 - (\epsilon-\mu)\mathbf{I} - 2\mathcal{G}_0^{-1}(i\omega_n) + [\mathbf{G}_c^0]^{-1}(i\omega_n)]^{-1}. \quad \text{(A1)}$$

One needs to carry out the integral for each ω_n. For the semicircular $D(\epsilon)$ given in Eq. (2)

$$D(\epsilon) = \frac{1}{2\pi t^2}\sqrt{4t^2-\epsilon^2}, \quad (|\epsilon| \le 2t), \quad \text{(A2)}$$

the exact integral formula is given in the following:

$$\int_{-\infty}^{\infty} d\epsilon \frac{D(\epsilon)}{\xi-\epsilon} = \begin{cases} \dfrac{\xi - \mathrm{Sgn}(\mathrm{Im}\ \xi)\sqrt{\xi^2-4t^2}}{2t^2}, & \mathrm{Im}\ \xi \neq 0, \\ \dfrac{\xi - \mathrm{Sgn}(\mathrm{Re}\ \xi)\sqrt{\xi^2-4t^2}}{2t^2}, & \mathrm{Im}\ \xi = 0 \ \text{and}\ |\xi| > 2t, \\ \dfrac{\xi}{2t^2}, & \mathrm{Im}\ \xi = 0 \ \text{and}\ |\xi| \leq 2t. \end{cases} \tag{A3}$$

In this equation, Im ξ and Re ξ are the imaginary and real parts of ξ. $\mathrm{Sgn}(x)=1$ and $\mathrm{Sgn}(x)=-1$ for x being a positive and a negative real number, respectively.

APPENDIX B: EFFECTIVE IMPURITY HAMILTONIAN AND ITS ACTION

The statistical action for the impurity model Eq. (10) reads

$$S_{imp} = \int_0^\beta d\tau \left[\sum_{k=1}^{B_s} \mathbf{a}_k^\dagger(\tau)\left(\frac{1}{2}\partial_\tau\sigma_3 + \mathbf{E}_k\right)\mathbf{a}_k(\tau) + \mathbf{b}_0^\dagger(\tau) \times \left(\frac{1}{2}\partial_\tau\sigma_3 - \frac{1}{2}\mu I\right)\mathbf{b}_0(\tau)\right] + \int_0^\beta d\tau \left[\sum_{k=1}^{B_s} [\mathbf{a}_k^\dagger(\tau)\mathbf{V}_k\mathbf{b}_0(\tau) + \mathbf{b}_0^\dagger(\tau)\mathbf{V}_k\mathbf{a}_k(\tau)] + \frac{U}{2}n_0(\tau)[n_0(\tau)-1] + \mathbf{\Phi}_0^\dagger(\tau)\mathbf{b}_0(\tau)\right]. \tag{B1}$$

The partition function can be expressed as the path integral over complex boson fields

$$Z = \int \mathcal{D}b_0^*(\tau)\mathcal{D}b_0(\tau) \int \prod_{k=1}^{B_s} \mathcal{D}a_k^*(\tau)\mathcal{D}a_k(\tau) e^{-S_{imp}}. \tag{B2}$$

Carrying out the Gaussian integral for the environmental degrees of freedom $\mathbf{a}_\mathbf{k}^\dagger$ and $\mathbf{a}_\mathbf{k}$, one obtains

$$Z = Z_a \int \mathcal{D}b_0^*(\tau)\mathcal{D}b_0(\tau) e^{-S_b}, \tag{B3}$$

where Z_a is the partition function of the bath degrees of freedom and the effective action S_b for the impurity is given by

$$S_b = \int_0^\beta d\tau \left\{ \mathbf{b}_0^*(\tau)\left[\frac{1}{2}\partial_\tau\sigma_3 - \frac{1}{2}\mu\mathbf{I} - \sum_{k=1}^{B_s}\mathbf{V}_k \times \left(\frac{1}{2}\partial_\tau\sigma_3 + \mathbf{E}_k\right)^{-1}\mathbf{V}_k\right] \times \mathbf{b}_0(\tau) + \frac{U}{2}n_0(\tau)[n_0(\tau)-1] + \mathbf{\Phi}_0^\dagger(\tau)\mathbf{b}_0(\tau)\right\}. \tag{B4}$$

Comparing this equation with the effective action derived from the cavity method Eq. (4), one gets

$$\mathcal{G}_0^{-1}(\tau-\tau') = -\left[\frac{1}{2}\partial_\tau\sigma_3 - \frac{1}{2}\mu\mathbf{I} - \sum_{k=1}^{B_s}\mathbf{V}_k \times \left(\frac{1}{2}\partial_\tau\sigma_3 + \mathbf{E}_k\right)^{-1}\mathbf{V}_k^\dagger\right]\delta(\tau-\tau'). \tag{B5}$$

Through this equation the Weiss field $\mathcal{G}_0^{-1}$ is related to the impurity parameters $\mathbf{E}_k$ and $\mathbf{V}_k$. After a Fourier transform, one gets Eq. (11).

APPENDIX C: LEHMANN REPRESENTATION OF THE BOSON GREEN'S FUNCTION

The boson GFs are calculated from their Lehmann representation after the eigenvalues and the eigenvectors are obtained by ED. In this appendix we present the corresponding Lehmann representations. The GFs are defined in Eq. (3) as

$$\mathbf{G}(\tau-\tau') \equiv -\langle T_\tau[\mathbf{b}(\tau)\mathbf{b}^\dagger(\tau')]\rangle = \begin{pmatrix} -\langle T_\tau[b(\tau)b^\dagger(\tau')]\rangle & -\langle T_\tau[b(\tau)b(\tau')]\rangle \\ -\langle T_\tau[b^\dagger(\tau)b^\dagger(\tau')]\rangle & -\langle T_\tau[b^\dagger(\tau)b(\tau')]\rangle \end{pmatrix} = \begin{pmatrix} G_1(\tau-\tau') & G_2(\tau-\tau') \\ G_3(\tau-\tau') & G_4(\tau-\tau') \end{pmatrix}. \tag{C1}$$

They have the symmetric relation $G_3(\tau-\tau')=G_2^*(\tau-\tau')$ and $G_4(\tau-\tau')=G_1^*(\tau-\tau')$. Here we only consider G_1 and G_2.

The diagonal GF is expressed as for $\omega_n \neq 0$,

$$G_1(i\omega_n) = -\frac{1}{2Z}\sum_{ij}\frac{e^{-\beta E_j}-e^{-\beta E_i}}{i\omega_n + (E_i-E_j)}\langle i|b|j\rangle\langle j|b^\dagger|i\rangle - \frac{1}{2Z}\sum_{ij}\frac{e^{-\beta E_i}-e^{-\beta E_j}}{i\omega_n + (E_j-E_i)}\langle i|b^\dagger|j\rangle\langle j|b|i\rangle \tag{C2}$$

and for $\omega_n=0$,

$$G_1(i0) = -\frac{1}{2Z}\sum_{E_i\neq E_j}\frac{e^{-\beta E_j}-e^{-\beta E_i}}{E_i-E_j}\langle i|b|j\rangle\langle j|b^\dagger|i\rangle - \frac{1}{2Z}\sum_{E_i\neq E_j}\frac{e^{-\beta E_i}-e^{-\beta E_j}}{E_j-E_i}\langle i|b^\dagger|j\rangle\langle j|b|i\rangle - \frac{\beta}{2Z}\sum_{E_i=E_j}e^{-\beta E_i}\langle i|b|j\rangle\langle j|b^\dagger|i\rangle - \frac{\beta}{2Z}\sum_{E_i=E_j}e^{-\beta E_i}\langle i|b^\dagger|j\rangle \times \langle j|b|i\rangle. \tag{C3}$$

Here, $Z=\Sigma_i \exp(-\beta E_i)$ is the partition function and $\beta=1/T$ the inverse temperature. The eigenvectors can be expanded by the basic vectors in the boson Fock space $\{|n\rangle\}$, $|i\rangle = \Sigma_n A_n^i |n\rangle$,

$$\langle i|b|j\rangle = \sum_{mn} A_n^{i*} A_m^j \langle n|b|m\rangle, \tag{C4a}$$

$$\langle j|b^\dagger|i\rangle = \sum_{mn} A_m^{j*} A_n^i \langle m|b^\dagger|n\rangle. \tag{C4b}$$

where $\langle n|b|m\rangle$ and $\langle m|b^\dagger|n\rangle$ are the matrix elements discussed in Eqs. (15) and (16). The coefficients A_n^i can be obtained from ED.

The off-diagonal GF reads for $\omega_n \neq 0$,

$$G_2(i\omega_n) = -\frac{1}{Z}\sum_{ij} \frac{e^{-\beta E_j} - e^{-\beta E_i}}{i\omega_n + (E_i - E_j)} \langle i|b|j\rangle\langle j|b|i\rangle, \tag{C5}$$

for $\omega_n = 0$,

$$G_2(i0) = -\frac{1}{Z}\sum_{E_i \neq E_j} \frac{e^{-\beta E_j} - e^{-\beta E_i}}{E_i - E_j} \langle i|b|j\rangle\langle j|b|i\rangle - \frac{\beta}{Z}\sum_{E_i = E_j} e^{-\beta E_i} \langle i|b|j\rangle\langle j|b|i\rangle. \tag{C6}$$

The disconnected GFs $\mathbf{G}_{dis}(i\omega_n)$ are defined as the sum over $E_i = E_j$ parts in Eqs. (C3) and (C6).

*nhtong@ruc.edu.cn

[1] D. Jaksch and P. Zoller, Ann. Phys. (N.Y.) **315**, 52 (2005).
[2] T. Matsubara and H. Matsuda, Prog. Theor. Phys. **16**, 416 (1956); **16**, 569 (1956); H. Matsuda and T. Matsubara, *ibid.* **17**, 19 (1957).
[3] D. Jaksch, C. Bruder, J. I. Cirac, C. W. Gardiner, and P. Zoller, Phys. Rev. Lett. **81**, 3108 (1998).
[4] I. Bloch, J. Dalibard, and W. Zwerger, Rev. Mod. Phys. **80**, 885 (2008).
[5] M. P. A. Fisher, P. B. Weichman, G. Grinstein, and D. S. Fisher, Phys. Rev. B **40**, 546 (1989).
[6] O. Mandel, M. Greiner, A. Widera, T. Rom, T. W. Hänsch, and I. Bloch, Nature (London) **425**, 937 (2003).
[7] A. Micheli, G. K. Brennen, and P. Zoller, Nat. Phys. **2**, 341 (2006).
[8] A. Smerzi and A. Trombettoni, Phys. Rev. A **68**, 023613 (2003).
[9] D. van Oosten, P. van der Straten, and H. T. C. Stoof, Phys. Rev. A **63**, 053601 (2001).
[10] K. Sheshadri, H. R. Krishnamurthy, R. Pandit, and T. V. Ramakrishnan, Europhys. Lett. **22**, 257 (1993).
[11] C. Pich and E. Frey, Phys. Rev. B **57**, 13712 (1998).
[12] P. Buonsante and A. Vezzani, Phys. Rev. A **70**, 033608 (2004).
[13] D. S. Rokhsar and B. G. Kotliar, Phys. Rev. B **44**, 10328 (1991).
[14] W. Krauth, M. Caffarel, and J. P. Bouchaud, Phys. Rev. B **45**, 3137 (1992).
[15] W. Krauth, Phys. Rev. B **44**, 9772 (1991).
[16] L. Amico and V. Penna, Phys. Rev. Lett. **80**, 2189 (1998).
[17] D. B. M. Dickerscheid, D. van Oosten, P. J. H. Denteneer, and H. T. C. Stoof, Phys. Rev. A **68**, 043623 (2003).
[18] Y. Yu and S. T. Chui, Phys. Rev. A **71**, 033608 (2005).
[19] C. Moseley, O. Fialko, and K. Ziegler, Ann. Phys. **17**, 561 (2008).
[20] J. K. Freericks and H. Monien, Europhys. Lett. **26**, 545 (1994).
[21] J. K. Freericks and H. Monien, Phys. Rev. B **53**, 2691 (1996).
[22] K. Sengupta and N. Dupuis, Phys. Rev. A **71**, 033629 (2005).
[23] N. Elstner and H. Monien, Phys. Rev. B **59**, 12184 (1999).
[24] F. E. A. dos Santos and A. Pelster, Phys. Rev. A **79**, 013614 (2009).
[25] M. Aichhorn, M. Hohenadler, C. Tahan, and P. B. Littlewood, Phys. Rev. Lett. **100**, 216401 (2008).
[26] B. Bradlyn, Francisco Ednilson A. dos Santos, and A. Pelster, Phys. Rev. A **79**, 013615 (2009).
[27] G. Semerjian, M. Tarzia, and F. Zamponi, Phys. Rev. B **80**, 014524 (2009).
[28] Y. Kato, Q. Zhou, N. Kawashima, and N. Trivedi, Nat. Phys. **4**, 617 (2008).
[29] G. G. Batrouni, R. T. Scalettar, and G. T. Zimanyi, Phys. Rev. Lett. **65**, 1765 (1990).
[30] S. Wessel, F. Alet, M. Troyer, and G. G. Batrouni, Phys. Rev. A **70**, 053615 (2004).
[31] M. Capello, F. Becca, M. Fabrizio, and S. Sorella, Phys. Rev. B **77**, 144517 (2008).
[32] G. Pupillo, C. J. Williams, and N. V. Prokof'ev, Phys. Rev. A **73**, 013408 (2006).
[33] B. Capogrosso-Sansone, N. V. Prokof'ev, and B. V. Svistunov, Phys. Rev. B **75**, 134302 (2007).
[34] B. Capogrosso-Sansone, S. G. Söyler, N. V. Prokof'ev, and B. V. Svistunov, Phys. Rev. A **77**, 015602 (2008).
[35] P. Pippan, H. G. Evertz, and M. Hohenadler, Phys. Rev. A **80**, 033612 (2009).
[36] R. V. Pai, R. Pandit, H. R. Krishnamurthy, and S. Ramasesha, Phys. Rev. Lett. **76**, 2937 (1996).
[37] T. D. Kühner and H. Monien, Phys. Rev. B **58**, R14741 (1998).
[38] N. D. Mermin and H. Wagner, Phys. Rev. Lett. **17**, 1133 (1966).
[39] G. E. Astrakharchik and S. Giorgini, Phys. Rev. A **68**, 031602(R) (2003).
[40] S. Wessel, F. Alet, S. Trebst, D. Leumann, M. Troyer, and G. G. Batrouni, J. Phys. Soc. Jpn. **74**, 10 (2005).
[41] F. Gerbier, Phys. Rev. Lett. **99**, 120405 (2007).
[42] M. Greiner, O. Mandel, T. Esslinger, T. W. Hänsch, and I. Bloch, Nature (London) **415**, 39 (2002).
[43] I. B. Spielman, W. D. Phillips, and J. V. Porto, Phys. Rev. Lett. **98**, 080404 (2007).
[44] T. Stöferle, H. Moritz, C. Schori, M. Köhl, and T. Esslinger, Phys. Rev. Lett. **92**, 130403 (2004).
[45] I. B. Spielman, W. D. Phillips, and J. V. Porto, Phys. Rev. Lett. **100**, 120402 (2008).
[46] S. Fölling, A. Widera, T. Müller, F. Gerbier, and I. Bloch, Phys. Rev. Lett. **97**, 060403 (2006).
[47] F. Gerbier, A. Widera, S. Fölling, O. Mandel, T. Gericke, and I. Bloch, Phys. Rev. A **72**, 053606 (2005).
[48] A. Griffin, Nat. Phys. **4**, 592 (2008).

[49] R. B. Diener, Q. Zhou, H. Zhai, and T. L. Ho, Phys. Rev. Lett. **98**, 180404 (2007).
[50] W. Metzner and D. Vollhardt, Phys. Rev. Lett. **62**, 324 (1989).
[51] A. Georges and G. Kotliar, Rev. Mod. Phys. **68**, 13 (1996).
[52] K. Byczuk and D. Vollhardt, Phys. Rev. B **77**, 235106 (2008).
[53] A. Hubener, M. Snoek, and W. Hofstetter, Phys. Rev. B **80**, 245109 (2009).
[54] H. J. Lee and R. Bulla, Eur. Phys. J. B **56**, 199 (2007).
[55] Y. Nambu, Phys. Rev. **117**, 648 (1960).
[56] D. Vollhardt, private communication.
[57] M. Caffarel and W. Krauth, Phys. Rev. Lett. **72**, 1545 (1994).
[58] R. Bulla, N. H. Tong, and M. Vojta, Phys. Rev. Lett. **91**, 170601 (2003); R. Bulla, H. J. Lee, N. H. Tong, and M. Vojta, Phys. Rev. B **71**, 045122 (2005); M. Vojta, N. H. Tong, and R. Bulla, Phys. Rev. Lett. **94**, 070604 (2005); N. H. Tong and M. Vojta, *ibid.* **97**, 016802 (2006).
[59] C. Zhang, E. Jeckelmann, and S. R. White, Phys. Rev. Lett. **80**, 2661 (1998).